

# A search for new hot subdwarf stars by means of Virtual Observatory tools II

E. Pérez-Fernández<sup>1,2\*</sup>, A. Ulla<sup>2</sup>, E. Solano<sup>3,4</sup>, R. Oreiro<sup>5</sup> and C. Rodrigo<sup>3,4</sup>

<sup>1</sup> IES de Beade, Consellería de Educación e O.U., Camiño de Outeiro 10, 36312 Vigo, Spain

<sup>2</sup> Departamento de Física Aplicada, Universidade de Vigo, Campus Lagoas-Marcosende, 36310 Vigo, Spain

<sup>3</sup> Departamento de Astrofísica, Centro de Astrobiología (INTA-CSIC), PO Box 78, E-28691 Villanueva de la Cañada (Madrid)

<sup>4</sup> Spanish Virtual Observatory

<sup>5</sup> Instituto de Astrofísica de Andalucía (IAA-CSIC), Glorieta de la Astronomía, s/n, 18008 Granada.

Accepted 2016 January 21; Received 2016 January 20; in original form 2015 July 6

## ABSTRACT

Recent massive sky surveys in different bandwidths are providing new opportunities to modern astronomy. The Virtual Observatory (VO) represents the adequate framework to handle the huge amount of information available and filter out data according to specific requirements.

In this work, we applied a selection strategy to find new, uncatalogued hot subdwarfs making use of VO tools. We used large area catalogues (GALEX, SDSS, SuperCosmos, 2MASS) to retrieve photometric and astrometric information of stellar objects. To these objects, we applied colour and proper motion filters, together with an effective temperature cut-off, aimed at separating hot subdwarfs from other blue objects such as white dwarfs, cataclysmic variables or main sequence OB stars. As a result, we obtained 437 new, uncatalogued hot subdwarf candidates. Based on previous results, we expect our procedure to have an overall efficiency of at least 80 per cent. Visual inspection of the 68 candidates with SDSS spectrum showed that 65 can be classified as hot subdwarfs: 5 sdOs, 25 sdOBs and 35 sdBs. This success rate above 95 per cent proves the robustness and efficiency of our methodology.

The spectral energy distribution of 45 per cent of the subdwarf candidates showed infrared excesses, a signature of their probable binary nature. The stellar companions of the binary systems so detected are expected to be late-type main sequence stars. A detailed determination of temperatures and spectral classification of the cool companions will be presented in a forthcoming work.

**Key words:** stars:early type – hot subdwarfs – Virtual Observatory tools – astronomical databases:miscellaneous

## 1 INTRODUCTION

Hot subdwarf (hot sd) stars are core-helium burning stars at the end of the horizontal branch or even beyond that stage. The origin of these faint, blue objects is still a matter of controversy. With effective temperatures exceeding 19000 K and  $\log g \geq 5$ , hot sds are objects that have lost most of their H envelope in previous evolutionary stages, leading to a  $\sim 0.5 M_{\odot}$  star. They are unable to follow canonical evolution through the Asymptotic Giant Branch (AGB) proceeding, instead, directly towards the white dwarf cooling track. Circumstances that lead to the removal of all but a tiny fraction of the hydrogen envelope, at about the same time as the core has achieved the mass required for the He flash ( $\sim 0.5 M_{\odot}$ ), are still a matter of debate. Theoretical evolution scenarios proposed so far include enhancement of the mass loss efficiency near the red giant branch (RGB) tip (D’Cruz et al. 1996) or mass transfer through

binary interaction (Mengel et al. 1976). See Heber (2009) for a review on observational and theoretical aspects of hot subdwarfs, or Geier (2013) for more recent discoveries.

Hot subdwarfs are found in the field, both in the disk and halo, but also populating the most Extreme part of the Horizontal Branch (EHB) of some Galactic clusters. Based on this observational evidence, they have been proposed as an explanation for the UV-upturn phenomenon shown in some elliptical galaxies (Brown et al. 1997).

Hot sds are divided in two main classes, sdBs and sdOs, according to composition. SdB spectra are dominated by the Balmer series, while sdOs are hotter objects characterized by the presence of He II 4686Å and the Pickering series. Additionally, a variety of He I lines may appear in both classes, and some sdOs show metallic C or N lines. More complex classification schemes have been proposed in Green, Schmidt & Liebert (1986) or more recently in Drilling et al. (2013).

The subdwarf database (Østensen 2006) catalogues 1600 sdBs

\* E-mail: estherperez@edu.xunta.es

and 500 sdOs spectroscopically confirmed hot subdwarfs. A significant number of new hot sds have been discovered in more recent studies like Vennes et al. (2011), Geier et al. (2011, 2015), Németh et al. (2012), Kleinman et al. (2013), Kupfer et al. (2015) or Kepler et al. (2016). Increasing the number of hot sds is important for a robust statistical confrontation with theoretical evolutionary scenarios. It may also lead to the discovery of interesting objects that are still scarce, such as pulsating sDBs or sdOs (Kilkenny 2002), eclipsing or reflecting hot sd binaries (For et al. 2010; Derekas et al. 2015), and hot sds as central stars of planetary nebulae (Aller et al. 2015). All of them are particularly interesting for studying the stellar interiors, the mass transfer mechanism at work, as well as the evolutionary formation channels, and would contribute to better understand these evolved objects.

Hot subdwarfs were first found analyzing faint blue stars, starting with the Humason & Zwicky (1947) survey or the Palomar-Green (PG) catalogue (Green et al. 1986). At present we have at our disposal deeper and more extensive surveys, covering large regions of the sky and wide spectral ranges. Besides, with online access tools like the Virtual Observatory (VO)<sup>1</sup> we can access data from most of these surveys in a very efficient way, crossmatching information to select objects with particular characteristics.

In this regard, the aim of the work here presented is to obtain a number of new hot sd candidates as large as possible. We apply the selection process developed in Oreiro et al. (2011) (hereafter paper I), that combines photometric and proper motion information from different surveys, making use of VO tools, with the intention of discriminating hot sds from other types of objects of similar colours, mainly white dwarfs (WD), cataclysmic variables (CV) and main-sequence O and B stars, considered as contamination sources in this work.

Section 2 describes the methodology employed, Section 3 the results obtained together with their analysis, Section 4 a summary of our main achievements on spectral classification of the new hot sd candidates discovered, and Section 5 ends with a general summary and conclusions.

## 2 METHODOLOGY

The methodology described in paper I is reproduced here. In that work, a hot sd selection procedure was defined and tested by means of a thorough retrieval, with the aid of VO tools, of multi-colour photometry and astrometric information from stellar catalogues. A filtering procedure to distinguish among different types of objects was designed to obtain a hot subdwarf sample with a low contamination factor. The method was tested on two sky regions: the Kepler FoV<sup>2</sup> and a region of  $300 \text{ deg}^2$  around  $(\alpha:225, \delta:5 \text{ deg})$  obtaining a high rate of success (above 80 per cent) in finding new uncatalogued hot subdwarfs. Temperatures were provided by fitting their spectral energy distribution (SED), and considering two-atmosphere fits for those objects with a clear infrared excess, a signature of the possible presence of a cool companion.

Once tested the validity of the proposed strategy, in this work we apply it to a wider sky region. The extension of this region is about  $11663 \text{ deg}^2$ , limited by the SDSS<sup>3</sup> DR7 survey coverage (Abazajian et al. 2009). Most of the Galactic northern cap down to  $b=+30$  is covered, as well as some strip-shaped areas crossing the

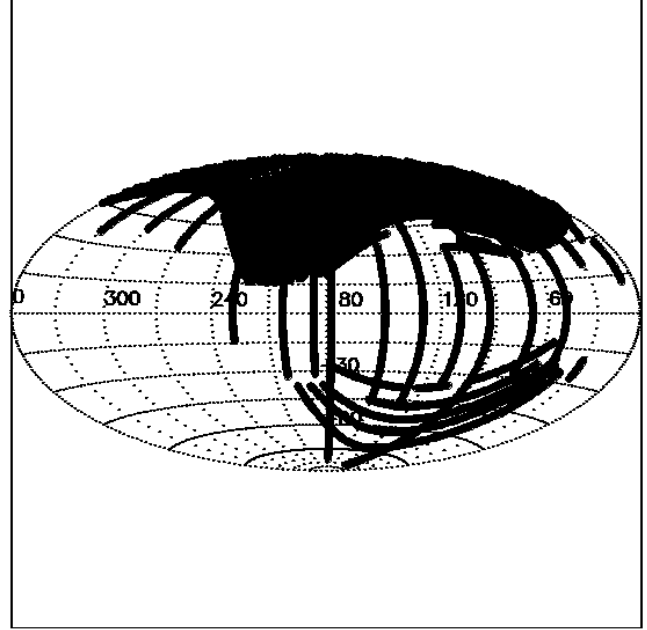


**Figure 1.** SDSS DR7 imaging coverage in Galactic coordinates, which is the region covered by this study. Source: <http://classic.sdss.org/dr7/coverage/>

Galactic plane and reaching the southern Galactic hemisphere. Fig. 1 shows the footprint in Galactic coordinates of the regions studied.

We remind the reader that the principal aim of this work is to apply a reliable selection procedure to find a large number of new hot subdwarf candidates, and not to perform a deep analysis of each star physical parameters. In this regard, we computed effective temperature estimates using an automated procedure provided by VOSA (Bayo et al. 2008), a very useful online facility of the Spanish Virtual Observatory<sup>4</sup>.

For the ease of the reader, we outline here the selection procedure.

• **Hot subdwarf selection filters:** First step was to crossmatch the photometric and proper motion surveys and apply to the retained sources the cuts aimed at selecting hot subdwarfs.

The surveys employed were SDSS DR7, GALEX GR6/GR7<sup>5</sup> (Bianchi & GALEX Team 2000), 2MASS Point Source Catalogue<sup>6</sup> (Skrutskie et al. 2006) and SuperCosmos<sup>7</sup> (Hambly et al. 2001). We required the GALEX sources to have measured magnitudes in both filters ( $FUV > 0$ ,  $NUV > 0$ ) and to be brighter than  $5\sigma$  of the magnitude limit ( $FUV < 19.9$ ,  $NUV < 20.8$ ). Sources must also be classified as point objects by SDSS ( $cl=6$ ). We retained sources with counterparts in all the surveys within a maximum distance of 5 arcsec. To the selected sources we applied the following cuts, as discussed in paper I:

$$-4 < (FUV_0 - K_{s0}) < 0.5 \quad (1)$$

$$-2 < (FUV_0 - NUV_0) < 0.2 \quad (2)$$

$$19 < H(NUV_0) < 27 \quad (3)$$

<sup>4</sup> <http://svo.cab.inta-csic.es>

<sup>5</sup> <http://galex.stsci.edu/>

<sup>6</sup> <http://www.ipac.caltech.edu/2mass/>

<sup>7</sup> <http://surveys.roe.ac.uk/ssa/>

<sup>1</sup> <http://www.ivoa.net/>

<sup>2</sup> <http://kepler.nasa.gov/science/about/targetFieldOfView/>

<sup>3</sup> <http://www.sdss.org/>

where the 0 subscript stands for Galactic extinction corrected magnitudes, and  $H(NUV_0)$  for the reduced proper motion of the  $NUV$  filter.

For bright stars, severe calibration problems in the GALEX photometry have been pointed out by Camarota & Holberg (2014) who, using a well studied sample of WDs with UV spectra, derived empirical corrections to the GALEX magnitudes in the non-linear range. The corrections are valid within the  $9.321 < NUV < 17.5$  or  $10.509 < FUV < 17.5$  ranges. We have thus identified the stars in our sample lying within those limits, and applied to them the correction factors established in that paper.

• **Discriminating new from already classified objects:** We crossmatched our list with published and well-established catalogues of spectroscopically confirmed subdwarfs, white dwarfs, cataclysmic variables and OB stars. These include:

- *The subdwarf database for hot sds* (Østensen 2006).
- *A selection of hot subluminous stars in the Galex survey* (Vennes et al. 2011; Németh et al. 2012)
- *The photometric and spectroscopic catalogue for luminous stars* (Reed 2005).
- *The catalogue of Cataclysmic Variables*, version 2006 (Downes et al. 2001).
- *The SDSS DR7 white dwarf catalogue* (Kleinman et al. 2013).
- *A Catalogue of Spectroscopically Identified White Dwarfs*, version 2008 (McCook & Sion 1999)

Sources already available in these catalogues were discarded. The remaining objects were searched in SIMBAD<sup>8</sup>, VIZIER<sup>9</sup> and any catalogue available through online VO tools. Very recent catalogues like Geier et al. (2015), Kupfer et al. (2015) and Gentile Fusillo et al. (2015) were considered in the Vizier search. Other catalogues containing spectroscopically confirmed hot subdwarfs but not included in Vizier (Vennes et al. 2011; Németh et al. 2012; Kawka et al. 2015; Kepler et al. 2016) were also inspected. Any source already spectroscopically classified in these catalogues was discarded.

• **Spectral distribution fit:** For each object in the pre-candidate list, we used VOSA to accomplish the following steps:

- Gathering of additional photometry: GALEX-SDSS-2MASS photometry was complemented with additional photometry from UKIDSS<sup>10</sup> LAS DR9 (Lawrence et al. 2007), Tycho-2 (Høg et al. 2000) and WISE<sup>11</sup> (Wright et al. 2010). Some candidates had saturated or bad SDSS photometry. In these cases we replaced SDSS by UCAC4 (Zacharias et al. 2013) photometry, if available.
- Magnitude-to-flux transformation: VOSA used the gathered photometric information to calculate the absolute fluxes and their associated errors taking advantage of the Filter Profile Service<sup>12</sup> (FPS), a service developed by the Spanish Virtual Observatory to provide VO access and representation of many of the most common photometric systems in astrophysics. Fluxes were then dereddened using the extinction law by Fitzpatrick (1999) and the  $E(B - V)$  values available in the GALEX catalogue, which

in turn have been taken from the Schlegel, Finkbeiner & Davis (1998) extinction maps.

– **Model comparison:** The flux-dereddened observational SEDs were then compared to the TLUSTY OS-TAR2002+BSTAR2006 NTLE models for O and B stars (Hubeny & Lanz 1995; Lanz & Hubeny 2003, 2007) implemented at VOSA to derive effective temperatures. We considered the whole model grid, with  $T_{\text{eff}}$  ranging from 15000 to 55000K. In the SEDs fitting procedure both surface gravity and metallicity were simply left as free parameters, as their impact on the effective temperature determination can be considered as negligible. Therefore, we warn the reader that the gravity and metallicity values obtained from the SED fitting cannot be considered as the real physical parameters of the objects listed in Tables 1 - 4 below.

Heber et al. (2000) have shown that the use of LTE vs NLTE model atmospheres yields almost identical  $T_{\text{eff}}$ 's and only systematic  $\log g$  differences, at least when fitting hot sd spectral lines. We do not expect other result in our procedure of fitting SEDs.

We have performed, anyway, a comparison between the effective temperatures calculated using the TLUSTY and Kurucz (Castelli et al. 1997) grids of atmospheric models. Only objects with a good SED fit flag (5XX) and a TLUSTY temperature value lower than 35000K (to avoid boundary problems with the maximum temperature of the grids) were considered. We obtained a difference in effective temperatures below 10 per cent for 90 per cent of the objects (or 82 per cent of objects for an up to 5 per cent difference), indicating that, as expected, the NLTE effects on  $T_{\text{eff}}$  determination can be neglected.

We also attempted to leave  $A_v$  as a free parameter in the SED fitting process. Nevertheless, due to the  $A_v - T_{\text{eff}}$  degeneracy, this exercise rendered multiple solutions and we finally decided to include extinction as a fixed parameter.

• **Source image checking:** Finally, we visually inspected using Aladin<sup>13</sup> the SDSS images and catalogue data of our pre-candidate list of targets to discard instrumental features, bad crossmatches or contamination from nearby, bright sources.

In fact, we found some cases with a clear mismatch between GALEX, SDSS and 2MASS sources. These pathological cases are mostly due to the different spectral coverage and limiting magnitude of the surveys. We kept these objects without infrared photometry in a separate list, as they appear to be very hot and blue objects, and thus interesting from our point of view (Table 4).

### 3 RESULTS

After crossmatching the photometric surveys and applying the selection filters in equations (1)-(3), we ended up with a list of 1242 pre-candidates. 638 of them were already classified in the literature, with the following percentages: 83 per cent hot subdwarfs, 12 per cent WD, 2 per cent CV, 2 per cent B stars, and less than 0.5 per cent other main sequence stars. These numbers agree with those obtained in paper I, demonstrating the robustness of our selection procedure. The remaining 604 pre-candidates were not found in the literature.

In Fig. 2 the classified and unclassified objects selected by the photometric and proper motion cuts are pictured in Galactic

<sup>8</sup> <http://simbad.u-strasbg.fr/simbad/>

<sup>9</sup> <http://vizier.u-strasbg.fr/viz-bin/VizieR>

<sup>10</sup> <http://surveys.roe.ac.uk/wsa/>

<sup>11</sup> <http://wise.ssl.berkeley.edu>

<sup>12</sup> <http://svo2.cab.inta-csic.es/theory/fps3/>

<sup>13</sup> <http://aladin.u-strasbg.fr/>

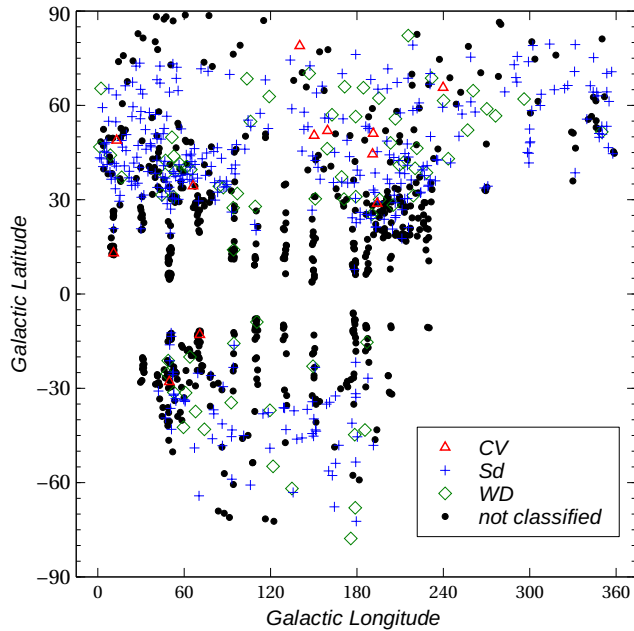


**Figure 2.** Galactic coordinates of the pre-candidates after the photometric and proper motion cuts. Those not yet classified in the literature are marked with black circles.

coordinates. Notice that a large fraction of the unclassified objects lay in the bands near the Galactic plane, as these tend to be less studied regions.

### 3.1 Effective temperatures

Effective temperatures were obtained from the comparison between the observational SEDs and the TLUSTY models. After the fitting, we kept candidates with  $T_{\text{eff}} > 19000\text{K}$ , provided that the fit was good. Sources with  $T_{\text{eff}} < 19000\text{K}$  and a bad SED fitting were also kept, as this could be a signal of a binary candidate. 167 out of the 604 unclassified sources did not pass the cut, leaving us with a list of 437 final subdwarf candidates.

The bad fits are of mainly three different sorts: excess in the red part of the spectrum (IR), ultraviolet (UV) excess, and both IR and UV excesses in the same source. IR excesses are probably a signature of a binary system. UV excess could also indicate the presence of a very hot companion, but uncertainties associated to the ultraviolet extinction correction cannot be discarded.  $E(B - V)$  values have been taken from Schlegel et al. (1998), who seem to overestimate the reddening to lines of sight where  $A_V \geq 0.5$  mag (Arce & Goodman 1999).

As a further check, we also performed in VOSA a Bayesian analysis of the model fits. We found that, for 356 sources, the probability associated to the  $T_{\text{eff}}$  value obtained from the chi-square fitting was over 80 per cent. For the rest of sources (81), we provide an effective temperature interval covering an accumulated probability of, at least, 80 per cent. With this procedure we obtain fairly temperature estimations for the whole sample. The only exception to this were the targets whose temperature estimate reached the upper limit of the TLUSTY models, 55000K. This is not surprising as we know that some sdOs can achieve very high temperatures (Stroeer et al. 2007). For these objects, just a lower limit in effective temperatures is provided.

To classify the quality of the fits we tagged each target with a

three digits quality flag (see Tables 1-4). The first digit ranges from one to five: ‘5’ represents good SED fitting, ‘4’ stands for excess in the red part of the SED (IR excess), ‘3’ for both IR and UV excesses, ‘2’ for UV excess only, and ‘1’ for a bad fitting of any other sort. Excesses in the infrared or ultraviolet part of the SED were defined whenever the relative difference between the model and observed (dereddened) values was above 20 per cent, and the difference increased with decreasing/increasing wavelength, for UV and IR, respectively. We found this criterion matched quite well with a visual inspection of the SED fits. Differences without a clear pattern, in the middle or any part of the SED, were considered bad fits of type ‘1’.

Second and third digits refer to the quality of the GALEX data: a ‘1’ in the second position represents a problematic GALEX artifact, and a ‘1’ in the third position stands for a bad flag in the photometry extraction<sup>14</sup>. In both cases, ‘0’ stands for a good GALEX flag. 2MASS quality flags were also considered: Photometric values with an *U* flag (*U* standing for *upper limit* in magnitude) were not taken into account to perform the SED fitting.

Examples of the different quality fits can be seen in Fig. 3. Red points (grey in the grey-scale version of the figure) represent the dereddened magnitudes of the given object and the connected blue points (dark grey) the synthetic magnitudes that best fit. Under each graph we represent the residuals of the observed data and models.

In Tables 1-4 we present a sample of the hot subdwarf candidates found by our selection method. Table 1 includes good fitted objects with photometric data ranging from the ultraviolet to the infrared, and thus represents clear single candidates (192 objects). Table 2 shows sources with excess in the red part of the SED, the most clear binary candidates (110 objects). In Table 3 we included the rest of the bad fitted objects (115). Finally, Table 4 includes hot objects with no infrared photometry available (20).

$T_{\text{eff}}$  estimates for candidates with flags 4XX, 3XX, 2XX and 1XX must be treated with caution, which is warned by means of one of these bad fit flags. We remind the reader that, although the estimated  $T_{\text{eff}}$  are below 19000K, these objects are kept in the candidate list because the combination of bad fit and low temperature is used as indicator for the presence of binary systems.

In all tables, *FUV* and *NUV* were taken from the GALEX archive, and corrected as explained above, if necessary; *u*, *g*, *r* are from SDSS Data Release 7 and *J*, *H*, *K* from the 2MASS Point Source Catalogue. We included a column with the 2MASS quality flags of the source.  $T_{\text{eff}}$  is obtained from the best SED fit performed by VOSA. As explained above, an interval in the temperature column is given whenever the Bayes analysis gave the most likely  $T_{\text{eff}}$  value with a probability below 80 per cent. The *fit flag* column shows our notation for the different qualities in the VOSA  $T_{\text{eff}}$  fit. In Tables 2 and 3 we also included the filter where the excess begins and the expected spectral type of the stellar companion, according to the criterium explained in the next section.

Full tables, with all the photometric filters and other data, including links to the SED fitting diagrams and the SDSS spectrum, when available, can be accessed using the SVO hot subdwarf archive (see Appendix A).

Fig. 4 shows a histogram of the effective temperatures obtained for both the good fitted single candidates (fit flag 5XX) and the most clear binary candidates (fit flag 4XX). The majority of stars within the single sample lay in the temperature range 20000-

<sup>14</sup> see the GALEX documentation at <http://galax.stsci.edu/GR6/?page=ddfaq#6>



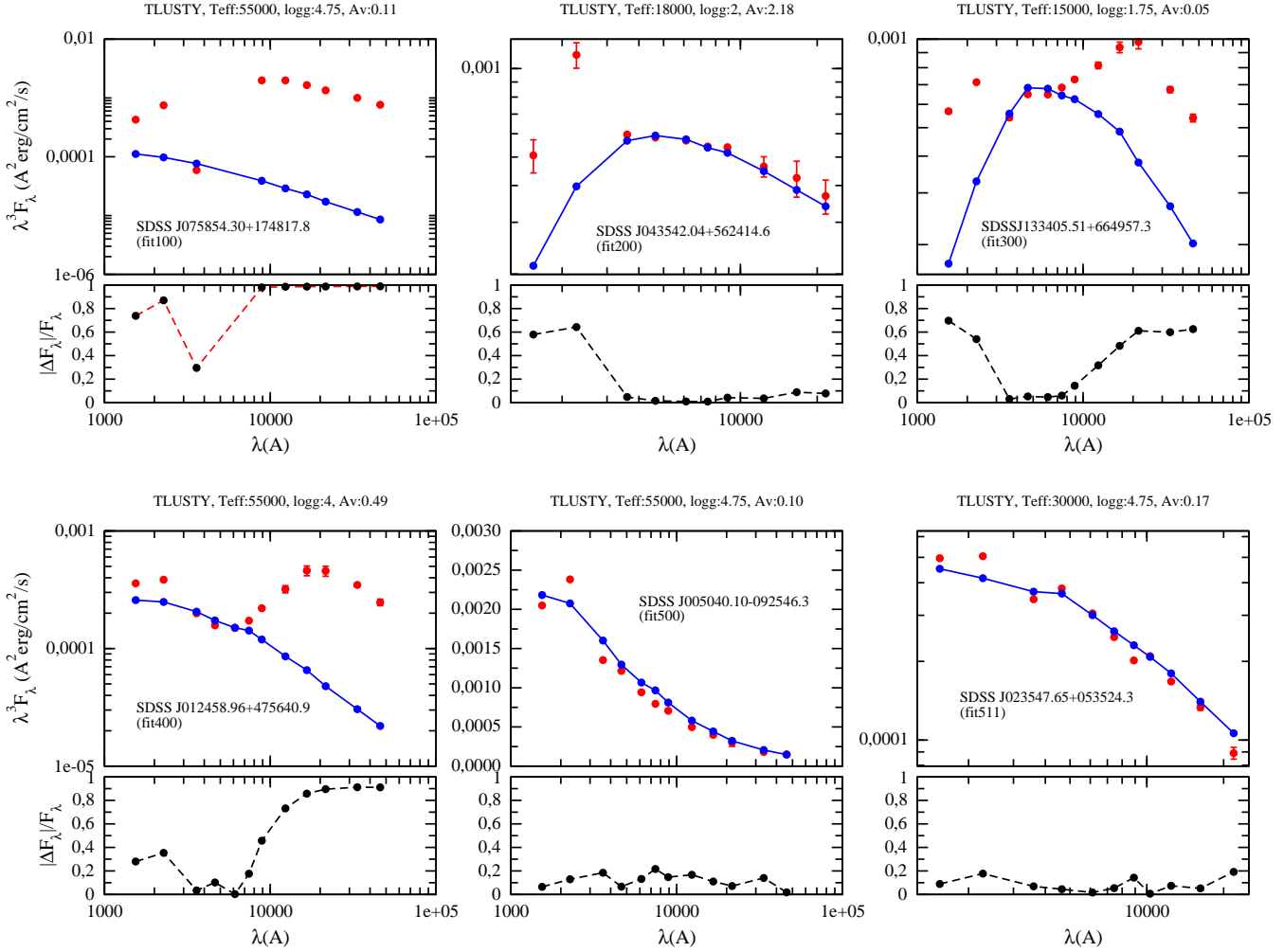


**Figure 3.** Examples of different quality SED fittings performed by VOSA. From left to right and up to bottom: bad fitting (flag 100), ultraviolet excess (flag 200), UV and IR excesses (flag 300), infrared excess (flag 400), good fitting (flag500) and good fitting with bad flags in GALEX photometry (flag 511). Red points (grey in the grey-scale version of the figure) represent the dereddened magnitudes of the given object, connected blue points (dark grey) the magnitudes given by the best fit model. Under each graph we represent the residuals of the observed data and models.

30000K while the effective temperatures of the binary sample are shifted towards lower values. This is not surprising, as we are including in the 4XX category objects with effective temperatures below 19000 K (see above). On the other hand, the peaks at 15000K and 55000K are signaling the limits in  $T_{\text{eff}}$  of the TLUSTY grid of models.

### 3.2 Binary sample

An important issue regarding hot subdwarfs is to know the binary fraction of these objects, as some of the proposed formation channels involve evolution in binary systems (Han et al. 2002, 2003; Clausen et al. 2012).

The three main binary evolution channels, as proposed in these papers, are the common envelope (CE) ejection channel, the stable Roche lobe overflow (RLOF) channel and the double helium white dwarfs (WDs) merger channel. The CE ejection channel leads to the formation of subdwarfs in short-period binaries with typical orbital periods between 0.1 and 10 days and very thin hydrogen-rich envelopes. On the other hand, the stable RLOF channel produces stars with long orbital periods (400 to 1500 days) and with

rather thick hydrogen-rich envelopes. The merger channel gives rise to single subdwarfs whose hydrogen-rich envelopes are extremely thin. This channel is believed to explain the formation of helium-rich hot subdwarfs (Zhang & Jeffery 2012).

Nevertheless, the contribution of the binary channels to the formation of the different subtypes of hot subdwarf stars is still unclear, with new discoveries challenging the standard binary evolution scenarios (see Geier 2013 for a recent review).

Regarding sdBs, the binary fraction is estimated around 40 per cent or higher, depending on the nature of the samples and the method used to detect the stellar companion (see Napiwotzki et al. 2004, or Heber 2009 for a review). In Lisker et al. (2005) the estimated binary fraction is 32 per cent, although this value should be taken as a lower limit as target selection was biased against composite spectrum objects. A recent study on IR excess in known radial velocity (RV) variable sdB binaries can be found in Kupfer et al. (2015).

The sdO binary fraction is more controversial, with different studies reaching opposite conclusions: Napiwotzki et al. (2004) found only one out of 23 RV variable sdO, while Green et al. (2008) and Geier et al. (2011) found a similar distribution of RV variations

**Table 1.** A sample of subdwarf candidates with good SED fit. *FUV* and *NUV* were taken from the GALEX archive (and corrected as explained in the text, if necessary); *u*, *g*, *r* are from SDSS Data Release 7 and *J*, *H*, *K* from the 2MASS Point Source Catalogue. We included the 2MASS quality flags of the source, where ‘U’ stands for upper limit in the corresponding photometric value.  $T_{\text{eff}}$  is obtained from the best SED fit performed by VOSA. An interval in the temperature column is given whenever the Bayes analysis gave the most likely  $T_{\text{eff}}$  value with a probability below 80 per cent. The last column represents a quality flag on the  $T_{\text{eff}}$  fit: ‘5’ in the first digit stands for good fitting; a ‘1’ in the second or third digit represents some problem in the GALEX photometry. The complete table can be found at <http://svo2.cab.inta-csic.es/vocats/hsa/>.

RA (J2000)	DEC (J2000)	NUV	FUV	u	g	r	J	H	K	2MASS flag	$T_{\text{eff}}$ (VOSA)	Fit flag
00:03:07	+24:12:12	16.028	15.916	16.105	16.148	16.533	16.628	16.085	17.106	BUU	25000	500
00:11:43	-10:40:34	14.044	13.947	14.686	14.987	15.471	15.95	15.601	16.524	ABU	32-35000	501
00:50:40	-09:25:46	12.845	12.553	13.818	14.174	14.716	15.216	15.307	15.402	AAC	55000	500
01:11:56	+15:17:53	14.866	14.499	15.154	15.206	15.627	15.74	15.948	15.615	ACD	25000	501
01:30:32	+52:33:50	16.679	16.402	16.072	16.067	16.18	15.931	15.965	15.998	ACD	37500	500
01:32:33	+51:57:57	15.281	15.309	14.935	14.996	15.167	15.202	15.186	15.291	AAB	37500	500
02:20:35	+17:04:07	14.912	14.615	15.011	14.957	15.274	15.241	15.103	14.992	AAC	24000	500
02:31:45	+22:08:30	16.749	16.597	16.545	16.392	16.646	16.319	16.277	15.914	ADD	23-24000	510
02:34:56	-06:09:13	14.884	14.167	15.604	15.963	16.475	16.888	16.566	16.862	CDU	42-55000	500
02:35:48	+05:35:24	14.725	14.269	15.407	15.518	15.999	16.806	16.327	15.609	CCU	30000	511

**Table 2.** A sample of hot subdwarf candidates with infrared excess in the SED fit. Column labels are like in Table 1. A value of ‘4’ in the first digit of the *Fit flag* column indicates the existence of excess in the red part of the SED. The beginning of the red excess (*Excess from* column) is obtained from the first band where the difference between the model and the dereddened observed value is above 20 per cent. The possible spectral type of the companion star is established by comparison with the Østensen (2006) subdwarf database (see Sec. 3.2). The complete table can be found at <http://svo2.cab.inta-csic.es/vocats/hsa/>.

RA (J2000)	DEC (J2000)	NUV	FUV	u	g	r	J	H	K	2MASS flag	$T_{\text{eff}}$ (VOSA)	Fit flag	Excess from	Binary class
00:14:40	+08:03:52	17.11	16.87	16.83	16.57	16.48	15.69	15.36	15.21	AAB	15000	410	z	GK
01:23:41	+30:02:32	16.02	15.62	16.33	16.35	16.64	16.42	15.84	15.29	BCU	18-21000	410	z	GK
01:24:59	+47:56:41	15.98	15.48	16.53	16.88	17.06	15.82	15.23	15.00	AAA	55000	400	i	FGK
01:33:14	+48:57:28	13.33	13.15	14.00	14.57	15.04	12.10	12.14	12.16	AAA	18000	410	B	F
02:28:23	+25:35:19	14.37	13.35	13.50	14.16	13.12	13.04	13.10	13.09	AAA	15000	400	B	F
02:41:13	+21:57:43	14.14	14.28	14.38	12.92	13.06	12.67	12.68	12.72	AAA	15000	400	B	F
02:44:14	+30:07:23	15.40	14.79	15.06	14.67	14.60	13.89	13.63	13.63	AAA	16000	400	i	FGK
02:57:48	+37:15:35	15.42	14.93	16.07	16.41	16.87	16.74	16.28	15.71	CDU	55000	400	J	GK
03:18:23	+41:55:22	14.36	13.99	14.49	14.63	14.92	14.69	14.52	14.34	AAA	40000	410	J	GK
03:48:30	+16:39:46	17.89	17.58	17.41	17.22	17.07	16.15	15.57	15.79	ABD	21000	410	i	FGK

between sdBs and sdOs. On the other hand, while Ulla & Thejll (1998) found that 6 out of 14 (43 per cent) new hot sdOs with IR excesses, Stroer et al. (2007) found 8 out of 52 (18 per cent) sdOs with photometric infrared excesses, although again this value should be taken as a lower limit.

A combination of optical and infrared photometry is commonly used to find late-type companions such as F, G or K types, because the hot subdwarf will shine in the blue, while the companion will have brighter red colours. Stark & Wade (2003) found a 40 per cent of binary systems in a magnitude-limited sample of hot subdwarfs from the Kilkeny catalogue (Kilkenny et al. 1988), using 2MASS infrared filters and Johnson or Strömgren optical photometry. In Girven et al. (2012) they also combine GALEX ultraviolet photometry with optical and infrared filters to select subdwarf candidates in double systems. They complete the photometric study with a spectroscopic classification, finding a large fraction of composite systems with F, G or K companions. On the other hand, detection of radial velocity variations in sdB stars is used to find close binaries with invisible companions such as white dwarfs (see for instance Morales-Rueda et al. 2003 and Copperwheat et al. 2011).

The photometric data of our sample ranges from the ultraviolet to the far infrared (WISE colours), which enabled us to detect flux excesses from the *B* magnitude. The companions found with our photometric methodology are expected to be late-type main sequence stars, such as F, G or K.

In our list of 437 hot subdwarf candidates, 20 of them have no infrared photometric data available (see Table 4). For the other 417, we consider as *binary candidates* those with quality SED fit 4 or 3 (IR or both IR and UV excess, Tables 2 and 3). There are 189 of them, making a total fraction of 45 per cent. This fraction could be overestimated, as some of the flux excesses may be apparent, due to inaccurate photometric measures or bad SED fittings.

The possible spectral type of the companion star was estimated analyzing the excess of hot sds with main sequence companions catalogued in Østensen (2006). We have selected all subdwarfs classified as sds+F, sds+G or sds+K of this catalogue and identified from which band the excess is detected in VOSA. Our criterion for the companion spectral type was the following:

- Excess from *B*, *V* or *g* band: type F (17 objects)
- Excess from *r* band: types F, G (6 objects)
- Excess from *i* band: types F, G, K (86 objects)
- Excess from *z* or *J* band: types G, K (69 objects)
- Excess from *H*, *Ks* or *W1* band: type K (11 objects)

Hot sds can have companions of other spectral types. Close binaries formed by cool main sequence M-type or substellar objects may alter the measured photometric values. The variation is due to a reflection effect in the light curve caused by the irradiated surface of the much cooler companion. It is estimated that only 1/5 of short period sdBs contain a dM (Østensen et al. 2013). In fact, few

**Table 3.** A sample of hot subdwarf candidates with bad SED fits. Column labels are like in Table 1. We include here bad fits with apparent UV excess ('2' as first digit in the *Fit flag* column), apparent excess in both UV and IR bands ('3' as first digit) and bad fits of any other sort ('1' as first digit). The complete table can be found at <http://svo2.cab.inta-csic.es/vocats/hsa/>

RA (J2000)	DEC (J2000)	NUV	FUV	u	g	r	J	H	K	2MASS flag	$T_{\text{eff}}$ (VOSA)	Fit flag
02:12:44	+68:07:08	19.267	18.996	19.312	19.065	18.758	15.598	14.956	15.017	ABC	15000	100
02:25:44	+72:49:44	18.642	17.982	16.902	16.125	15.575	14.055	13.661	13.361	AAA	29-37500	200
02:27:18	+73:36:11	17.864	17.382	16.32	15.454	14.907	13.483	12.976	12.969	AAA	19000	200
02:51:46	+75:09:04	19.360	19.049	18.504	18.023	17.711	16.597	15.767	15.942	BUU	15000	200
03:33:56	+17:56:36	17.699	17.156	17.975	18.011	18.26	16.703	15.656	16.914	BUU	18000	300
03:53:07	+16:48:49	15.646	15.113	15.036	14.675	14.598	13.577	13.11	13.046	AAA	15000	300
04:07:24	+14:44:06	18.995	18.562	17.535	16.905	16.51	15.156	14.639	14.566	AAA	15000	300
04:31:18	+55:53:08	18.696	18.598	17.365	17.054	16.889	15.899	15.531	15.277	ABB	37500	200
04:35:42	+56:24:15	19.770	19.514	18.022	17.523	17.105	15.931	15.644	15.444	ABC	18000	200
04:38:22	+19:03:06	17.079	16.814	16.619	16.34	16.283	15.546	15.14	15.003	AAB	18000	310
04:41:41	-06:11:29	15.389	15.132	15.735	15.54	15.614	15.061	14.833	14.867	AAB	15000	300

**Table 4.** Hot subdwarf candidates without infrared photometric data. We include here sources with good fit ('5' as first digit in the *Fit flag* column), apparent UV excess ('2' as first digit), and bad fits of any other sort ('1' as first digit).

RA (J2000)	DEC (J2000)	NUV	FUV	u	g	r	$T_{\text{eff}}$ (VOSA)	Fit flag
02:51:03.80	+75:15:03.4	16.7211	16.3976	17.243	17.194	17.564	42500	200
04:55:29.84	+24:45:07.6	18.8049	18.0702	18.501	18.631	18.853	42500	201
04:59:12.49	+60:51:56.5	19.0112	18.7774	19.017	18.631	18.929	37500	200
04:59:39.94	+59:48:53.5	17.5742	17.1230	17.219	17.25	17.56	42500	100
05:02:51.04	+13:49:26.9	20.4623	19.3643	19.512	19.522	19.552	42500	200
05:11:25.05	+15:03:01.0	18.9370	18.3932	17.986	18.012	18.026	40000	500
06:11:51.35	+34:04:01.5	19.3621	19.2375	19.924	20.152	20.544	42500	200
06:25:53.27	+34:54:28.2	16.8423	16.4591	17.304	17.298	17.666	42500	210
06:40:51.07	+26:44:28.0	12.9711	13.1221	13.524	11.024	11.064	15000	100
08:00:03.16	+07:40:43.3	14.6031	13.9893	15.507	15.907	16.432	55000	501
08:06:08.31	+10:24:20.1	16.4314	16.1312	17.044	17.195	17.682	28000	500
08:13:32.86	+05:54:30.1	14.8425	14.1695	15.608	16.093	16.639	55000	500
08:23:15.22	+00:18:46.0	15.6761	15.0236	16.502	17.019	17.385	55000	500
08:28:16.33	+22:32:26.5	14.3126	13.6464	13.754	12.389	12.777	15000	400
16:07:41.25	+25:42:20.6	16.4320	16.1035	16.825	16.971	17.423	28000	500
17:37:03.25	+50:40:41.1	15.4195	15.2508	15.982	16.041	16.539	27000	500
20:14:55.06	+08:42:13.9	18.8628	18.5533	19.143	19.03	19.424	30000	500
20:46:23.13	-06:59:26.8	16.4524	15.9148	17.081	17.455	17.89	55000	500
21:08:04.46	+05:15:28.5	16.2921	15.8421	16.777	17.042	17.462	42500	500
23:28:59.74	+52:16:24.1	18.4366	18.0371	18.742	18.888	19.255	42500	200

reflecting sdBs+dM/BD systems are known, and they show typical peak-to-peak photometric amplitudes of  $\sim 0.2$  mag or less, diminishing towards blue wavelengths. This effect is not expected to significantly alter our procedure.

Less common are hot subdwarfs in eclipsing binaries, either with dM/BD or WD companions (see For et al. (2010)). In these cases, deep eclipses with  $\sim < 0.8$  mag variations occur (although see the extraordinary sdO+dM system in Derekas et al. (2015)). A raw estimate of the number of eclipsing sdB+dM systems in our sample leads to a negligible number of photometric disturbances caused by photometry being acquired on eclipse-phase. Of course, we can not rule out that chances of this effect occur, which could explain any of the bad fits encountered in this work.

A more rigorous check of all possible binary candidates, using a two-component fit, is presently being addressed, and will be presented in a future work.

### 3.3 Colour-colour diagrams

Colour-colour or colour-magnitude diagrams allow us to separate sources of different nature using photometric colours. This is commonly used to detect ultraviolet or infrared excesses signaling a probable binary nature of the objects under study.

We have first plotted our candidates in the colour-colour plane  $u_0 - FUV_0$  versus  $V_0 - u_0$ , as seen in Fig. 5. The 0 subscript stands for dereddened magnitudes, with the  $E(B - V)$  values taken from Schlegel et al. (1998), and the corresponding correction factors computed from the formulae in Cardelli, Clayton & Mathis (1989).  $FUV$  and  $u$  are GALEX and SDSS filters, respectively. As we do not have data of the  $V$  magnitude for all our candidates, we use a  $V$  value computed with the transformation formula given in Jester et al. (2005) between the  $ugriz$  and  $UBV$  systems:

$$V = g - 0.58(g - r) - 0.01 \quad (4)$$

The figure shows the relative difference in the blue colours of our candidates. Most of the good fitted objects lay on the right side of the diagram, as would be expected, because they stand for relatively hot single candidates. The bluer stars lay on the bottom right

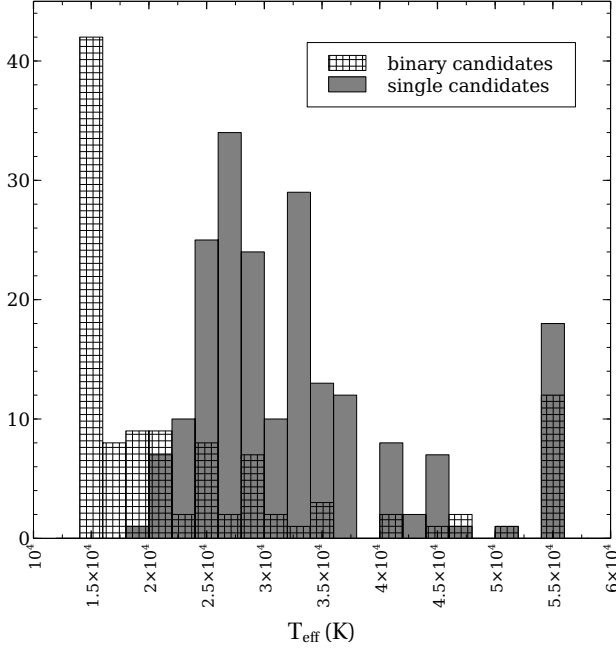


**Figure 4.** Effective temperature histogram for single (fit flag 5XX) and binary (fit flag 4XX) candidates. The two peaks at 15000 and 55000K show the boundary effects of the TLUSTY models limits (see 3.1 for more details).

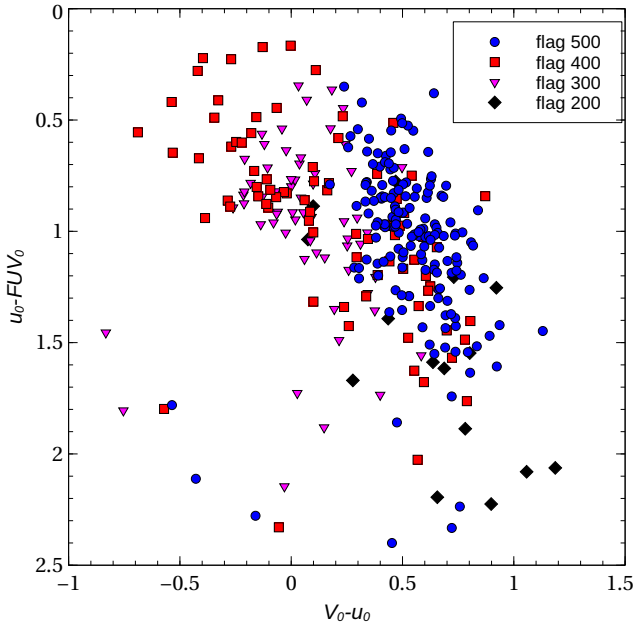


**Figure 5.** The relative difference in blue colours of our candidates is visible in this plane. The bluer stars lay on the bottom right corner.

corner of the diagram, where we can see objects labeled with ultra-violet excess (quality fit 200). To discard the UV excess was only an effect of a possible overestimation in the extinction correction, we checked the  $A_V$  values of these objects. They turned up to be relatively high ( $A_V > 1.14$  mag), but not higher than many other objects without UV excess (single or binary candidates).

There are various references in the recent literature studying

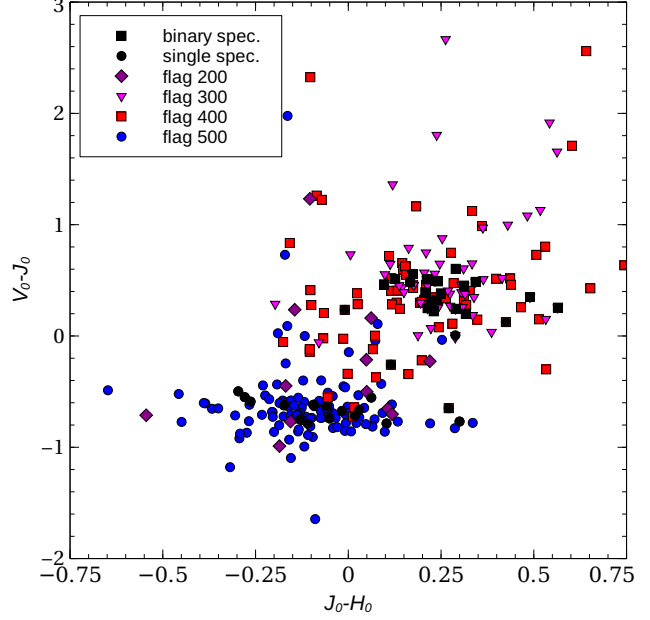


**Figure 6.** An analogous of the gap in Green et al. (2008) is presented here. Single subdwarf candidates (flag 500) concentrate in the bottom-left of the diagram, while composite candidates (flag 400 and 300) are in the upper right side. We also represent the binaries and single objects spectroscopically identified using SDSS spectra (see Sect. 4).

different samples of hot subdwarfs and proposing alternative ways to separate single from binary stars using colour-colour diagrams. In Stark & Wade (2003) they plot  $J - K_s$  versus  $V - K_s$  and found single stars remain inside a box limited by  $V - K_s \leq +0.2$  and  $J - K_s \leq +0.05$ , while the composite stars lay outside this rectangle (see fig. 1 in that paper). In Green et al. (2008) they plot  $V - J$  versus  $J - H$  of a sample of confirmed subdwarfs, finding a gap in the colour diagram, separating single from composite stars (fig.5 of that paper). Finally, in Girven et al. (2012)  $FUV - r$  is plotted versus  $r - K_s$ , showing also separate regions for the single and composite subdwarfs.

Similarly to Green et al. (2008), to show the single or binary nature of our candidates we plotted  $V_0 - J_0$  versus  $J_0 - H_0$ , the  $V$  magnitude computed as in equation (4) and  $J$  and  $H$  from 2MASS. The result is shown in Fig. 6.

Not all the candidates are represented there. Many of our sources are quite faint in the infrared, and thus do not have very good 2MASS flags: 173 sources (41 per cent) have at least an  $U$  (*upper limit*) in one of the 2MASS filters; while other 46 sources (11 per cent) have at least one filter with a  $D$  or  $E$  flag<sup>15</sup>. To avoid big errors, we restricted our plot to sources with  $err(J) + err(H) < 0.3$ . For the rest of the objects, we substituted 2MASS data with UKIDSS, if available.

In Fig. 6, we can see that single candidates tend to concentrate around  $V_0 - J_0 \approx -0.6$ , and binary candidates, although more spread, around  $V_0 - J_0 \approx 0.25$ . In spite of the source spreading, the gap between composite and single systems is still visible. The source spreading may be due to a variety of factors. We first noted that the majority of binary candidates spread around the diagram

<sup>15</sup> [http://www.ipac.caltech.edu/2mass/releases/allsky/doc/sec1\\_6b.html](http://www.ipac.caltech.edu/2mass/releases/allsky/doc/sec1_6b.html) gives detailed explanations of their quality flags.



are those where the excess begins at  $B$  or  $r$  magnitudes, causing the optical region of the SED to be untypical. Other uncertainties in the SDSS photometry, due to either faint magnitudes or bright values near the saturation limits, could cause the star to be misplaced. Finally, we can not discard other phenomena, like the presence of planetary nebulae.

#### 4 SPECTRAL CLASSIFICATION

A first classification scheme for hot subdwarfs was proposed in Green et al. (1986), where an eight class system was defined. In Drilling et al. (2013) an evolved MK-like system is developed. In this system hot subdwarfs are divided in four sequences: *He-weak*, *He-normal*, *He-strong* and *He-strong C*, with carbon or other metallic lines. The differences in helium content of each object are also quantified measuring ratios of hydrogen to helium line depths. In each of the four helium sequences, the spectral subclasses would range from sdO1 to sdB9, as in the MK system, line depths and ratios varying smoothly within each sequence (see figs. 1 to 4 in that paper). Stars former classified within the somehow *ad-hoc* sdOB subclass (Moehler et al. 1990) are placed naturally in this scheme, in the transition between late sdO and early sdB subclasses. In the present work we will apply the Drilling et al. (2013) system to classify the candidates with spectrum.

Only 68 stars of our list of subdwarf candidates (16 per cent) had SDSS spectrum. We begun with a visual inspection of each object's whole spectrum. One spectrum was too noisy to allow identification. The rest were identified as one white dwarf, one probable cataclysmic variable and 65 subdwarfs: 5 sdOs (8 per cent), 25 sdOBs (38 per cent) and 35 proper sdBs (54 per cent). Note the effectiveness of our selection procedure improves to 95.6 per cent within this subset.

We also inspected the presence of characteristic lines of cooler main sequence stars, to identify binary candidates. In particular, we looked for the Mg I triplet (5172, 5183, 5167Å), the G band (4300Å), and the Ca II K line (3933Å). The Na I doublet (5889-5895Å) can also be an indicator, although it may be overlapped with a near He II line. We found 23 probable binary systems: 22 binary sdBs (including sdOBs) and 1 binary sdOs. The binary fraction for sdBs obtained by visual inspection of the spectrum was of 37 per cent, somehow lower than the photometric fraction. Besides the possible overestimation of the photometric fraction, as argued above, the relatively low signal-to-noise ratio of some SDSS spectra may be obscuring the binary nature of some candidates, hiding the cold companion lines. We point out that all the spectrum-detected binary systems are also binary candidates from the photometric excess point of view.

To classify the subdwarfs within the Drilling et al. (2013) system we cut and normalized the spectra between 4000 and 5000 Å and then compared them with the standard stars defining the system. The complete classification of our candidates can be found in the electronic tables. A sample is shown in Figures 7-8. Summarizing our results, we have found:

- 1 star (1.5 per cent) belonging to the *He-strong C* sequence,
- 2 stars (3.1 per cent) in the *He-strong* sequence,
- 48 stars (73.9 per cent) in the *He-normal* sequence and
- 14 stars (21.5 per cent) in the *He-weak* sequence.

Note that the signal-to-noise ratio of some spectra might be masking weak metallic carbon or nitrogen lines, affecting the *He-strong C* and *He-strong* relative abundances.

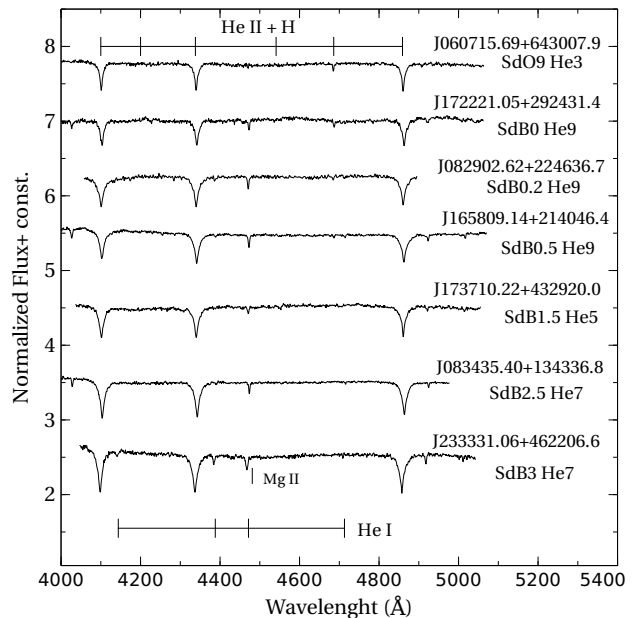


**Figure 7.** Subdwarfs in the *He-normal* spectral sequence, following Drilling et al. (2013). Star identifications are taken from SDSS.

Calibrations made in Drilling et al. (2013) demonstrate that *He-weak* stars have subsolar helium abundances, *He-normal* stars more nearly solar abundances and *He-strong* objects high helium abundances. The problem of helium abundances in hot subdwarfs has been addressed in O'Toole (2008) and Geier et al. (2013). In Edelman et al. (2003) a correlation between effective temperature and helium abundance in sdB stars was discovered, showing two sequences with approximately the same trend with increasing  $T_{\text{eff}}$  (fig. 5 in that paper). The ratio of objects in the lower sequence to those in the upper one is argued to be between 1:10 and 4:10 in O'Toole (2008). Our ratio 14:48 of weak to normal helium stars is consistent with these margins.

Drilling et al. (2013) suggest their spectral sequences are temperature sequences, and find linear trends plotting the effective temperature against the spectral class (fig. 10 and 11 in that paper). For a check, we plotted our good SED fitted candidates in the  $T_{\text{eff}}$ -spectral class plane, together with Drilling et al. (2013) linear regressions. As a result, and although our temperatures appear in general subestimated, we found our candidates from classes sdO9 to sdB3 to roughly follow Drilling et al.'s trend lines. On the contrary, the hotter sdO3-sdO7 classes do not seem to follow this behavior. Such a result is not surprising, due to the effective temperature upper limit of the TLUSTY models (55000K).

#### 5 CONCLUSIONS

In this work we have extended the selection procedure developed in Oreiro et al. (2011) to identify hot subdwarfs, taking advantage of Virtual Observatory tools. The selection procedure includes photometric and proper motions filters and an effective temperature cut-off. We have identified 437 new subdwarf candidates from a 11663  $\text{deg}^2$  sky region, limited by the SDSS DR7 image coverage. We expect an effectiveness of at least 80 per cent, although the subsample of objects with SDSS spectra reached a subdwarf identification above 95 per cent, proving the accuracy of our selection filters.

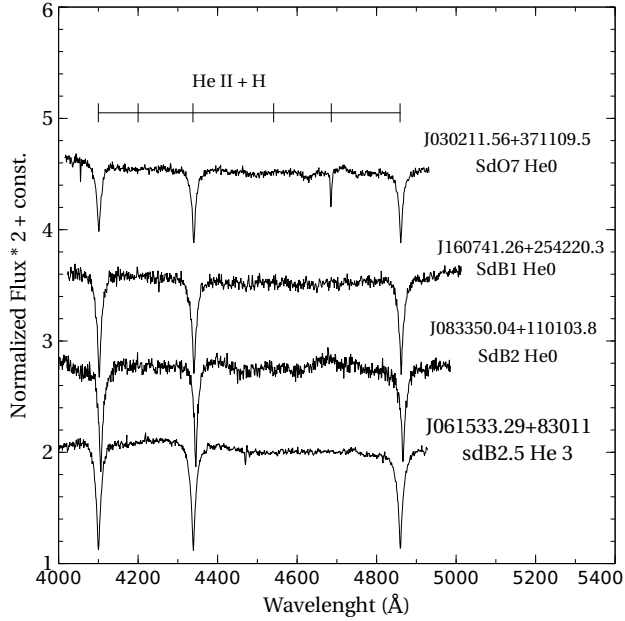


**Figure 8.** Subdwarfs in the *He-weak* spectral sequence, following Drilling et al. (2013). Star identifications are taken from SDSS.

From our spectral energy distribution analysis, we have estimated a photometric binary fraction of 45 per cent, while identification of cool star metallic lines in the spectra yields a 37 per cent of binaries among this subsample. Both numbers, although rough estimates, are in agreement with previous studies. Our method mainly selects binaries with late-type main sequence stellar companions, like F, G or K.

The colour-colour diagrams of Fig. 5 and 6 show the difference in, respectively, the blue and red colours of our subdwarf candidates. Objects in the lower right corner of Fig. 5 show a clear ultraviolet excess (labeled with SED fitting flag 200 – see text for details). In Fig. 6 we see a clear clustering of the single candidates around  $V_0 - J_0 \approx -0.6$ , and the colour gap between single and binary subdwarfs discovered in Green et al. (2008) is reproduced.

We have also performed a detailed spectral classification of the 68 candidates with SDSS spectra, following a recent MK-like system for hot subdwarfs developed by Drilling et al. (2013). We found our candidates perfectly suit in one of the four helium sequences proposed in that paper.

Much work remains to be done after the selection procedure developed here. Regarding the list of hot subdwarf candidates, a deeper analysis of the binary sample is presently under study. A two-body SED fitting will yield temperature values of the cold companion, which will aid to estimate its spectral class and its distance. As argued in Clausen et al. (2012), composite systems of the type sdB + early F could be crucial in determining the binary formation channel of hot subdwarfs, depending on the periods measured for these systems. Recently, in Barlow et al. (2013) and Vos et al. (2013), long period sdB+F/G systems have been reported. It would thus be interesting to know if our sample contains this type of binaries, and to make a follow-up study of them, determining their orbital parameters.

Both the twenty candidates without available infrared photometry and the seventeen objects with apparent ultraviolet excess are very interesting from our point of view, as good candidates for very hot objects. The hotter sDOs are measured to have up to

100000K effective temperatures (Stroeer et al. 2007). These objects are scarce between subdwarfs, and some of them have been proved to have planetary nebulae (Aller et al. 2013, 2015), a signal of a probable post AGB origin (Heber 1991). Photometric and spectroscopic accurate data would be needed to reach further conclusions about the origin of these stars.

Finally, a detailed line spectral analysis of the hot subdwarf candidates, to be performed using advanced/accurate NLTE atmospheric models, would yield more reliable values for the star effective temperatures, helium abundances and surface gravities. The position of our candidates in the  $T_{\text{eff}} - \log g$  plane would contribute to discriminate between the different origins and evolution paths proposed for hot subdwarfs.

Regarding the search of new hot subdwarf candidates, different approaches could be used. One of those would imply applying our selection procedure to new releases of some of the surveys already considered (e.g. SDSS, GALEX) or using new catalogues, both in the optical (e.g. Pan-Starrs, or J-PAS in the near future) and in the infrared (UKIDSS, VISTA).

Another possibility would be employing other catalogues containing astrometric information. At this moment, our routine discards any source without proper motion data in the SuperCosmos survey. This fact could be modified making the routine look for proper motion information in other catalogues, like UCAC4 or PP-MXL (Roeser, Demleitner & Schilbach 2010).

It would also be interesting to explore the possibilities of the data that GAIA<sup>16</sup> would provide regarding this point. GAIA would measure distances with great accuracy, giving us information of star luminosities and their position in the HR diagram. This would yield estimations of both star masses and ages, an important information to track the evolutionary paths of hot subdwarfs.

Attention must be paid as well to other forthcoming missions such as CHEOPS (Fortier et al. 2014) or PLATO (Rauer et al. 2014), as they are expected to have an impact on ultra-high precision photometry and stellar astroseismology for bright targets, covering large fractions of the sky (up to 50 per cent in the case of PLATO), and widening, then, the possible detection of new pulsating hot sd.

## ACKNOWLEDGEMENTS

We thank A. Aller for helping us improving the spectra classification. This publication makes use of VOSA, developed under the Spanish Virtual Observatory project supported from the Spanish MICINN through grant AyA2011-24052. It has also been partially supported by grant INCITE09312191PR (which includes FEDER funds), given by the Xunta de Galicia, and by grant 12VI20, given by the Universidade de Vigo. This research has made use of the SIMBAD database, the Vizier catalogue access tool (originally published in Ochsenbein, Bauer & Marcout 2000) and the *Aladin sky atlas*, all operated at CDS, Strasbourg, France.

## REFERENCES

- Abazajian K. N. et al., 2009, *ApJS*, 182, 543
- Aller A., Miranda L. F., Olguín L., Vázquez R., Guillén P. F., Oreiro R., Ulla A., Solano E., 2015, *MNRAS*, 446, 317
- Aller A. et al., 2013, *A&A*, 552, A25

<sup>16</sup> <http://sci.esa.int/gaia/>

- Arce H. G., Goodman A. A., 1999, *ApJ*, 512, L135
- Barlow B. N., Liss S. E., Wade R. A., Green E. M., 2013, *ApJ*, 771, 23
- Bayo A., Rodrigo C., Barrado y Navascués D., Solano E., Gutiérrez R., Morales-Calderón M., Allard F., 2008, *A&A*, 492, 277
- Bianchi L., GALEX Team, 2000, *Mem. Soc. Astron. Italiana*, 71, 1123
- Brown T. M., Ferguson H. C., Davidsen A. F., Dorman B., 1997, *ApJ*, 482, 685
- Camarota L., Holberg J. B., 2014, *MNRAS*, 438, 3111
- Cardelli J. A., Clayton G. C., Mathis J. S., 1989, *ApJ*, 345, 245
- Castelli F., Gratton R. G., Kurucz R. L., 1997, *A&A*, 318, 841
- Clausen D., Wade R. A., Kopparapu R. K., O’Shaughnessy R., 2012, *ApJ*, 746, 186
- Copperwheat C. M., Morales-Rueda L., Marsh T. R., Maxted P. F. L., Heber U., 2011, *MNRAS*, 415, 1381
- D’Cruz N., Rood R., O’Connell R., Dorman B., Dickens R., 1996, in *Bulletin of the American Astronomical Society*, Vol. 28, American Astronomical Society Meeting Abstracts, p. 1390
- Derekas A. et al., 2015, preprint (arXiv:1505.06487)
- Downes R. A., Webbink R. F., Shara M. M., Ritter H., Kolb U., Duerbeck H. W., 2001, *PASP*, 113, 764
- Drilling J. S., Jeffery C. S., Heber U., Moehler S., Napiwotzki R., 2013, *A&A*, 551, A31
- Edelmann H., Heber U., Hagen H.-J., Lemke M., Dreizler S., Napiwotzki R., Engels D., 2003, *A&A*, 400, 939
- Fitzpatrick E. L., 1999, *PASP*, 111, 63
- For B.-Q. et al., 2010, *ApJ*, 708, 253
- Fortier A., Beck T., Benz W., Broeg C., Cessa V., Ehrenreich D., Thomas N., 2014, in *Society of Photo-Optical Instrumentation Engineers (SPIE) Conference Series*, Vol. 9143, Society of Photo-Optical Instrumentation Engineers (SPIE) Conference Series, p. 2
- Geier S. et al., 2011, *A&A*, 530, A28
- Geier S., 2013, in *European Physical Journal Web of Conferences*, Vol. 43, p. 4001
- Geier S., Heber U., Edelmann H., Morales-Rueda L., Kilkeny D., O’Donoghue D., Marsh T. R., Copperwheat C., 2013, *A&A*, 557, A122
- Geier S. et al., 2015, *A&A*, 577, A26
- Gentile Fusillo N. P., Gänsicke B. T., Greiss S., 2015, *MNRAS*, 448, 2260
- Girven J. et al., 2012, *MNRAS*, 425, 1013
- Green E. M., Fontaine G., Hyde E. A., For B.-Q., Chayer P., 2008, in *Astronomical Society of the Pacific Conference Series*, Vol. 392, Hot Subdwarf Stars and Related Objects, Heber U., Jeffery C. S., Napiwotzki R., eds., p. 75
- Green R. F., Schmidt M., Liebert J., 1986, *ApJS*, 61, 305
- Hambly N. C. et al., 2001, *MNRAS*, 326, 1279
- Han Z., Podsiadlowski P., Maxted P. F. L., Marsh T. R., 2003, *MNRAS*, 341, 669
- Han Z., Podsiadlowski P., Maxted P. F. L., Marsh T. R., Ivanova N., 2002, *MNRAS*, 336, 449
- Heber U., 1991, in *IAU Symposium*, Vol. 145, Evolution of Stars: the Photospheric Abundance Connection, Michaud G., Tutukov A. V., eds., p. 363
- Heber U., Reid I. N., Werner K., 2000, *A&A*, 363, 198
- Heber U., 2009, *ARA&A*, 47, 211
- Høg E. et al., 2000, *A&A*, 357, 367
- Hubeny I., Lanz T., 1995, *ApJ*, 439, 875
- Humason M. L., Zwicky F., 1947, *ApJ*, 105, 85
- Jester S. et al., 2005, *AJ*, 130, 873
- Kawka A., Vennes S., O’Toole S., Németh P., Burton D., Kotze E., Buckley D. A. H., 2015, *MNRAS*, 450, 3514
- Kepler S. O. et al., 2016, *MNRAS*, 455, 3413
- Kilkenny D., 2002, in *Astronomical Society of the Pacific Conference Series*, Vol. 259, IAU Colloq. 185: Radial and Nonradial Pulsations as Probes of Stellar Physics, Aerts C., Bedding T. R., Christensen-Dalsgaard J., eds., p. 356
- Kilkenny D., Heber U., Drilling J. S., 1988, *South African Astronomical Observatory Circular*, 12, 1
- Kleinman S. J. et al., 2013, *ApJS*, 204, 5
- Kupfer T. et al., 2015, *A&A*, 576, A44
- Lanz T., Hubeny I., 2003, *ApJS*, 146, 417
- Lanz T., Hubeny I., 2007, *ApJS*, 169, 83
- Lawrence A. et al., 2007, *MNRAS*, 379, 1599
- Lisker T., Heber U., Napiwotzki R., Christlieb N., Han Z., Homeier D., Reimers D., 2005, *A&A*, 430, 223
- McCook G. P., Sion E. M., 1999, *ApJS*, 121, 1
- Mengel J. G., Norris J., Gross P. G., 1976, *ApJ*, 204, 488
- Moehler S., Richtler T., de Boer K. S., Dettmar R. J., Heber U., 1990, *A&AS*, 86, 53
- Morales-Rueda L., Maxted P. F. L., Marsh T. R., North R. C., Heber U., 2003, *MNRAS*, 338, 752
- Napiwotzki R., Karl C. A., Lisker T., Heber U., Christlieb N., Reimers D., Nelemans G., Homeier D., 2004, *Ap&SS*, 291, 321
- Németh P., Kawka A., Vennes S., 2012, *MNRAS*, 427, 2180
- Ochsenbein F., Bauer P., Marcout J., 2000, *A&AS*, 143, 23
- Oreiro R., Rodríguez-López C., Solano E., Ulla A., Østensen R., García-Torres M., 2011, *A&A*, 530, A2
- Østensen R. H., 2006, *Baltic Astronomy*, 15, 85
- Østensen R. H. et al., 2013, *A&A*, 559, A35
- O’Toole S. J., 2008, in *Astronomical Society of the Pacific Conference Series*, Vol. 392, Hot Subdwarf Stars and Related Objects, Heber U., Jeffery C. S., Napiwotzki R., eds., p. 67
- Rauer H. et al., 2014, *Experimental Astronomy*, 38, 249
- Reed C., 2005, *VizieR Online Data Catalog*, 5125, 0
- Roeser S., Demleitner M., Schilbach E., 2010, *AJ*, 139, 2440
- Schlegel D. J., Finkbeiner D. P., Davis M., 1998, *ApJ*, 500, 525
- Skrutskie M. F. et al., 2006, *AJ*, 131, 1163
- Stark M. A., Wade R. A., 2003, *AJ*, 126, 1455
- Stroeer A., Heber U., Lisker T., Napiwotzki R., Dreizler S., Christlieb N., Reimers D., 2007, *A&A*, 462, 269
- Ulla A., Thejll P., 1998, *A&AS*, 132, 1
- Vennes S., Kawka A., Németh P., 2011, *MNRAS*, 410, 2095
- Vos J., Østensen R. H., Németh P., Green E. M., Heber U., Van Winckel H., 2013, *A&A*, 559, A54
- Wright E. L. et al., 2010, *AJ*, 140, 1868
- Zacharias N., Finch C. T., Girard T. M., Henden A., Bartlett J. L., Monet D. G., Zacharias M. I., 2013, *AJ*, 145, 44
- Zhang X., Jeffery C. S., 2012, *MNRAS*, 419, 452

## APPENDIX A: THE SVO HOT SUBDWARF ARCHIVE

In order to help the astronomical community on using the catalogue of subdwarfs identified in this paper we have developed an archive

system that can be accessed from a Web page<sup>17</sup> or through a Virtual Observatory ConeSearch<sup>18</sup>

### A1 Web access

The archive system implements a very simple search interface that permits queries by coordinates/radius as well as by other criteria of interest (object identifier, Teff, quality flag or excess). A selection of the astrometric, photometric and physical parameters to be displayed in the table of results can also be done assigning a type of verbosity: minimum, medium or maximum. The default search radius is set to 5 arcsec. The user can also select the maximum number of sources to return (with values ranging from 10 to unlimited) (Fig. A1).

The result of the query is a HTML table with all the sources found in the archive fulfilling the search criteria. Detailed information on the output fields can be obtained placing the mouse over the name of the column. The archive implements the SAMP (Simple Application Messaging Protocol). SAMP allows applications to communicate with each other in a seamless and transparent way for the user. This way, the results of a query can be easily transferred to other VO application, such as Topcat (Fig A2).

### A2 Virtual Observatory access

The Virtual Observatory (VO)<sup>19</sup> is an international initiative whose primary goal is to provide an efficient access and analysis of the information hosted in astronomical archives and services. Having a VO-compliant archive is an important added value for an astronomical project to guarantee the optimum scientific exploitation of their datasets.

Our archive system has been designed following the IVOA standards and requirements. In particular, it implements the Cone Search protocol, a standard defined for retrieving records from a catalogue of astronomical sources. The query made through the Cone Search service describes a sky position and an angular distance, defining a cone on the sky. The response returns a list of astronomical sources from the catalogue whose positions lie within the cone, formatted as a VOTable.

<sup>17</sup> <http://svo2.cab.inta-csic.es/vocats/hsa/>

<sup>18</sup> Try for instance <http://svo2.cab.inta-csic.es/vocats/hsa/cs.php?RA=0&DEC=0&SR=100&VERB=2>

<sup>19</sup> <http://www.ivoa.net>



## The SVO hot subdwarf archive



Home Data retrieval News Documentation Coverage Map Help-Desk

RA (?) DEC (?) Radius (?) Search Reset

180 : : 0 : : 180 : : 10 results minimum verb. (Maximum Search Radius allowed: 180 degrees)

☒ Don't restrict coordinates

[\[-\] Hide additional search fields](#)

objID (?)

SDSS\_name (?)

Teff (chi2-VOSA) (?) - -

Fit\_flag (?) - - - -

Start\_excess (?)

- List of hot subdwarf candidates with good SED fit (table 1 in Pérez-Fernández et al).
- List of hot subdwarf candidates with infrared excess in the SED fit (table 2 in Pérez-Fernández et al).
- List of hot subdwarf candidates with bad SED fits (table 3 in Pérez-Fernández et al).
- List of hot subdwarf candidates without infrared photometry (table 4 in Pérez-Fernández et al).

Figure A1. Web interface. Input query form

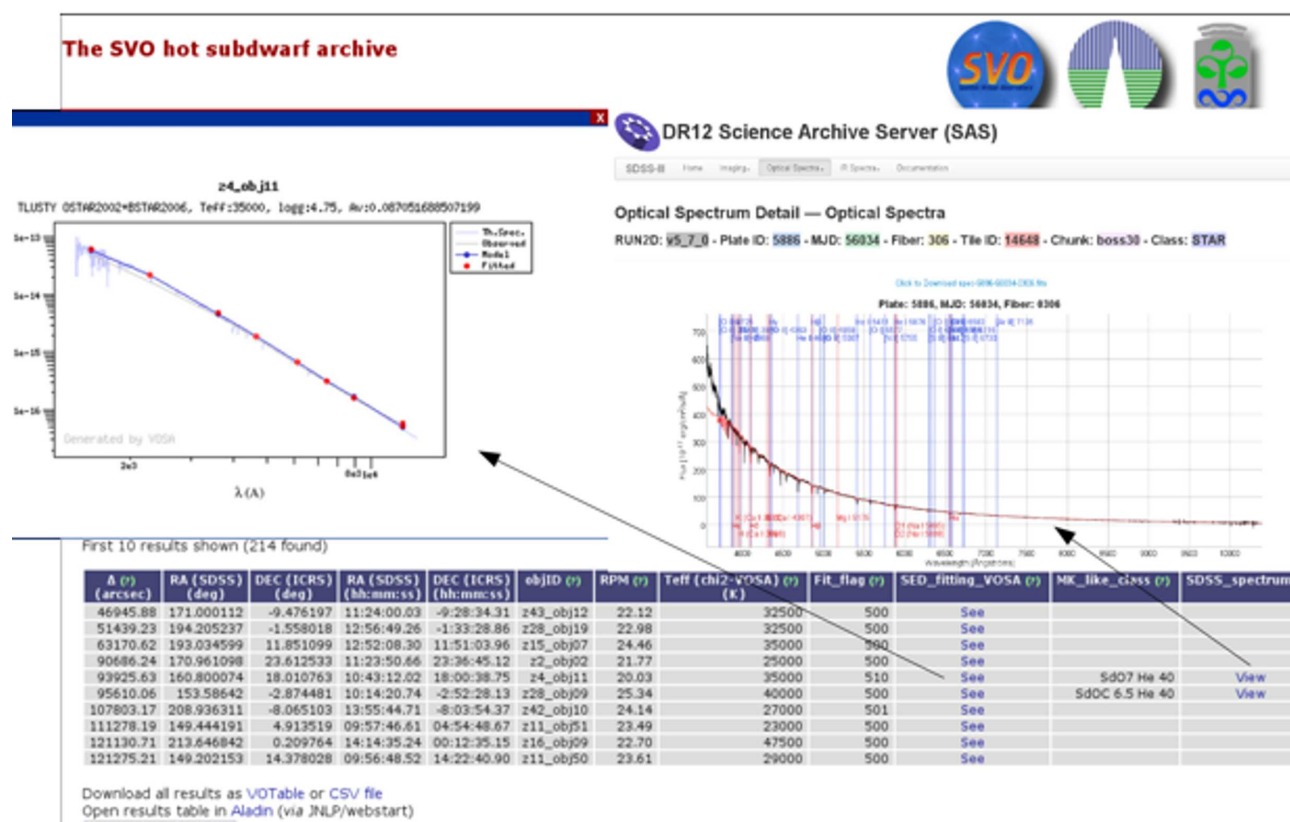


Figure A2. Result from a query. The SED and SDSS spectrum visualisation capabilities are also shown